

A bottom-up optimization method for inverse design of two-dimensional clamped-free elastic rods

Longhui Qin^{1,2} | Jianxiong Zhu¹ | Weicheng Huang^{1,3}

¹School of Mechanical Engineering,
Southeast University, Nanjing, People's
Republic of China

²State Key Laboratory of Fluid Power and
Mechatronic Systems, Zhejiang
University, Hangzhou, China

³Jiangsu Engineering Research Center of
Aerospace Machinery, Southeast
University, Nanjing, People's Republic of
China

Correspondence

Weicheng Huang, School of Mechanical
Engineering, Southeast University,
Nanjing 211189, China.
Email: weichenghuang@seu.edu.cn

Funding information

Natural Science Foundation of Jiangsu
Province; Open Foundation of the State
Key Laboratory of Fluid Power and
Mechatronic Systems

Abstract

Rod-like structures, such as DNA, climbing plants, and cables, pervade the nature and our daily life and also belong to a frequently encountered engineering problem, which usually assume a deformed shape based on the competition between elasticity (stretching, bending, twisting) and external forces (e.g., gravity). These structures often undergo geometrically nonlinear deformation under its own weight. Computing the natural (undeformed) shape of a rod from the observed deformed configuration is a nonlinear inverse problem. Here we introduce a numerical method to solve this problem in case planar (2D) rods, that is, beams, under a clamped-free boundary condition. A simulation model is developed based on the discrete elastic rods (DER) algorithm to address the forward deformation process from natural to deformed shapes under gravity. Based on the internal mechanical link among the nodes on the discretized elastic rod, a bottom-up optimization method is proposed in this article for an efficient inverse solution. Associated with it, a global searching algorithm is developed to search for the optimal bending curvature along the arc length of the rod. The method is numerically validated for accuracy and sheds light on the inverse design of rod-like structures for various applications, for example, soft robots and tails of animated characters.

KEY WORDS

bottom-up design method, discrete elastic rods, global searching algorithm, inverse design, solid mechanics

1 | INTRODUCTION

Rod-like structures are ubiquitous in nature, industry, and our daily life, such as DNA molecules, tendrils, hairs and soft robots.^{1–5} What they appear in real world are usually deformed shapes resulting from stretching, bending, and twisting under external forces or constraints, for example, gravity. Numerous works have explored this forward deformation process and relevant mechanics.^{6–10} Inversely, how to compute the natural geometries (original or undeformed curve) and material parameters given the deformed configuration is also significant in the design and fabrication of composite structures, 3D or 4D printing, and soft robotics.^{11–15}

Plenty of analytical and numerical models have been developed to simulate the forward process, that is, from original to deformed shape. For example, a discrete deformable model was developed by Bertails et al.³ to predict the dynamics of natural hair; each strand was represented by a piecewise helical rod and animated using the principles of Lagrangian

mechanics. An analytical continuum mechanical model of an elastic composite tube was introduced by Wada¹⁶ to determine the equilibrium helical shapes of thin elastic composites. Gazzola et al.¹⁷ developed a numerical method based on the Cosserat rod model to simulate the dynamics of filaments that were considered as slender cylindrical structures. Lazarus et al.¹⁸ and Su et al.¹⁹ employed discrete numerical models and experiments to explore the deformation and buckling of slender rods resulting from a complex interplay between geometrical constraints, elasticity, and weight. A number of works explored the stability of two-dimensional and three-dimensional elastic rods.^{20,21} These researches on the forward process lay a foundation for the inverse design that we address in this article.

Although a handful of recent works addressed the inverse problem of deformed rod,^{22–26} most of them contributed to parameter (e.g., bending stiffness) identification in an inverse way. A well-posed convex second-order cone quadratic program was solved by Derouet-Jourdan et al.²² to obtain the frictional contact forces in dynamic hair modeling. In this article, the hair-body and hair-hair contact were incorporated and the motion of hair appeared more natural and smooth. Given the deflection of the action point of a concentrated load, the inverse problem studied by Zhang and Yang²³ was to determine value of the load for a variable-arc length beam, whose analytical solutions were found via a set of nonlinear equations. Based on a discrete-structure simulation, Reference 24 inversely estimated the effective constitutive law from the deformation data and thus improved the continuum-rod model for microfilaments. However, very few works could be found to explore the whole undeformed geometries of elastic rods when a deformed configuration is given. An asymptotic numerical method was proposed by Chen²⁵ to search for the inverse elastic shape, where gravity was iteratively changed step-by-step. Compared with classic iterative methods, the computational time was greatly reduced. Prediction accuracy was closely related to the maximum number of iterations and more computation time was required for relatively soft elastic rods that undergo large deformation. Very recent work by Bertails-Descoubes et al.²⁷ proved the uniqueness of the inverse natural shape for thin elastic rods, the solution of which could be computed by solving in sequence three linear initial value problems.

In this article, focusing on two-dimensional clamped-free elastic rods (i.e., its one end is clamped while the other end free), we propose a numerical method to find the inverse solution—the undeformed natural shape—given the target deformed shape. A simulation model is implemented based on the discrete elastic rods (DER) algorithm—an efficient simulation tool for rod-like structures^{28–30}—for the forward process of an undeformed rod transitioning to a deformed shape under gravity. Different from various existing discrete models,^{31,32} it considers stretching, bending and twisting energies while Bishop frame and material frame are utilized to update the deformation process at each time step.^{28,30} Although heuristic optimization algorithms, for example, simulated annealing (SA), genetic algorithm (GA), and particle swarm optimization (PSO), are widely utilized to solve the inverse design problem,^{33–35} they require long computational time. Moreover, in this problem, we observe that the error between a guessed solution and the true solution does not monotonically decrease as the number of unknown variables is reduced. A bottom-up design method based on a global searching algorithm is proposed leveraging the internal mechanical link (force and moment balance) between consecutive edges to gradually solve from the last edge to the first. Several representative natural curves are used to verify the effectiveness of the proposed bottom-up design method. Due to our application of a nondimensional parameter arising from the competition of bending and gravitational energies, the method is robust against material parameters and the magnitude of acceleration due to gravity.

In the next section, the problem of interest will be described in detail with the forward and inverse process clarified. The bottom-up optimization method and the global searching algorithm are then elucidated in Section 3, followed by a discussion on the existence of inverse solution. The entire method will be validated in Section 4. Section 5 contains a discussion on the results and existing limitations.

2 | PROBLEM DESCRIPTION

2.1 | Forward process

Among a variety of simulation techniques, we choose DER algorithm as the basis to develop the planar deformation model since it is not only accurate in simulating geometrically nonlinear deformation process of elastic rods but also computationally efficient.²⁹ In DER, dynamic relaxation method is used to solve nonlinear problems very efficiently, for example, automatic capture of bifurcation and buckling. Moreover, absolute nodal coordinate formulation is adopted in DER, with which more complex models could be introduced more conveniently. As a dynamic model, it proves

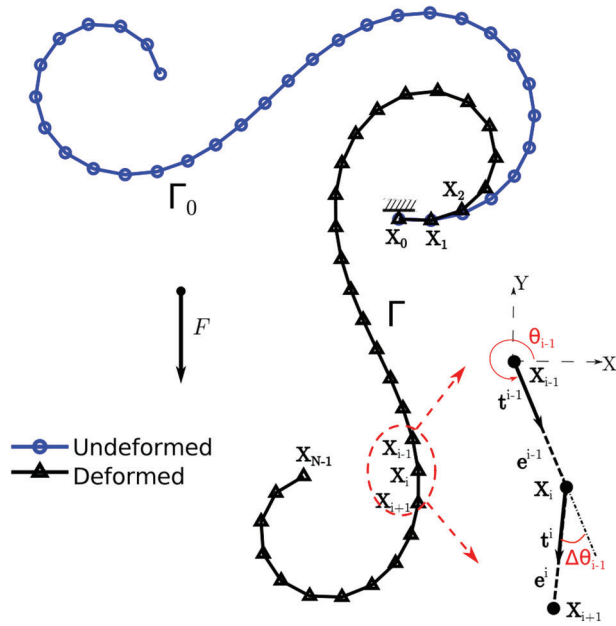


FIGURE 1 Schematic of the deformation process under external force F implemented by our developed planar simulation model based on DER. An amplified figure shows the geometrical representation in details. Therein θ_{i-1} is the orientation angle of edge e^{i-1} while $\Delta\theta_{i-1}$ is the turning angle between edge e^{i-1} and e^i

excellent in solving geometrically nonlinear static problems.^{28,29,36} As shown in Figure 1, an elastic rod is discretized into N nodes \mathbf{X}_i ($i = 0, \dots, N - 1$) connecting $N - 1$ edges $\mathbf{e}^i = \mathbf{X}_{i+1} - \mathbf{X}_i$ ($i = 0, \dots, N - 2$). The vector \mathbf{t}^i is an unit vector along edge \mathbf{e}^i such that $\mathbf{t}^i = \frac{\mathbf{e}^i}{\|\mathbf{e}^i\|}$, θ_i —referred to as the orientation angle—is the signed angle from the x -axis to \mathbf{t}^i , and the turning angle $\Delta\theta_{i-1}$ is the signed angle from \mathbf{t}^{i-1} to \mathbf{t}^i . The edges constitute the discrete representation of the centerline of the rod. In the 3D version of DER, each edge is decorated with a material frame and the rotation of this frame with respect to the tangent is represented by a scalar twist angle. Based on the balance of the elastic forces (e.g., bending, twisting and stretching) and external forces (e.g., gravity), $4N - 1$ equations of motion for $4N - 1$ degrees of freedom ($3N$ nodal coordinates and $N - 1$ twist angles) are established. Shape of the elastic rod (represented by the degrees of freedom) and the velocity at each node can be computed by solving this system of second order ordinary differential equations.

Specifically, the total potential of a 2D rod system is a sum of elastic stretching and bending,

$$E_s = \sum_{i=0}^{N-2} \frac{1}{2} EA (\epsilon^i)^2 \|\bar{\mathbf{e}}^i\| \quad (1)$$

$$E_b = \sum_{i=1}^{N-2} \frac{1}{2} EI(\kappa_i)^2 \frac{1}{\Delta\bar{l}_i}, \quad (2)$$

where $\epsilon^i = \|\mathbf{e}^i\|/\|\bar{\mathbf{e}}^i\| - 1$ is the stretching strain of i th edge, $\kappa_i = 2 \tan(\Delta\theta_i/2)$ is the bending curvature at i th node, $\Delta\bar{l}_i = (\|\bar{\mathbf{e}}^i\| + \|\bar{\mathbf{e}}^{i-1}\|)/2$ is the Voronoi length, and a bar on top indicates the evaluation in the undeformed configuration. $EA = \pi Er_0^2$ is stretching stiffness and $EI = \frac{\pi}{4}Er_0^4$ is bending stiffness (as for circular cross-section).

The final equilibrium configuration of a rod is derived through a dynamic relaxation method. At each time step, with the degrees of freedom (DOF) vector, \mathbf{q}_k (where DOF vector is the sum of total node coordinates, $\mathbf{q} = [\mathbf{x}_0, \mathbf{x}_1, \dots, \mathbf{x}_{N-1}]$), and its velocity, $\dot{\mathbf{q}}_k$, the dynamic governing equation of a rod system can be expressed as:

$$\mathbb{M}\Delta\mathbf{q}_{k+1} - h\mathbb{M}\dot{\mathbf{q}}_k - h^2 \left(\mathbf{F}_{k+1}^{\text{internal}} + \mathbf{F}_{k+1}^{\text{damping}} + \mathbf{F}_{k+1}^{\text{gravity}} \right) = \mathbf{0}, \quad (3a)$$

$$\mathbf{q}_{k+1} = \mathbf{q}_k + \Delta\mathbf{q}_{k+1}, \quad (3b)$$

$$\dot{\mathbf{q}}_{k+1} = \frac{1}{h} \Delta\mathbf{q}_{k+1}, \quad (3c)$$

where the diagonal mass matrix \mathbb{M} is time-independent, $\mathbf{F}^{\text{internal}} = -\partial(E_s + E_b)/\partial \mathbf{q}$ is the internal elastic force, $\mathbf{F}^{\text{damping}}$ is the damping force, and $\mathbf{F}^{\text{gravity}}$ is the gravitational force. h is the time step size and the subscript $k+1$ (and k) represents the quantity at time t_{k+1} (and t_k). Although this type of discrete simulation is established for dynamic system, it is still valid for the equilibrium configuration under arbitrary loading and boundary conditions when the viscosity is introduced into the system as a part of external force, known as dynamic relaxation method.

As the equilibrium configuration is required (a specific solution \mathbf{q} that satisfies $\mathbf{F}^{\text{internal}} = \mathbf{F}^{\text{gravity}}$), the diagonal mass matrix as well as the damping force doesn't contribute to the static results, and the effective physical parameters are rod length L , rod radius r_0 , Young's modulus E , and external force $\mathbf{F}^{\text{gravity}}$. Considering what is involved in this article is the slender structure ($L \gg r_0$), the stretching stiffness is much larger than the bending stiffness and EA performs as a Lagrange multiplier to ensure the uniaxial stretching strains remain to be zeros. Therefore, the external gravitational force is balanced with internal bending force and the nondimensional form is

$$\mathbf{F}^{\text{gravity}} \sim \mathbf{F}^{\text{gravity}} L^2/EI. \quad (4)$$

Other parameters, for example, stretching strain ϵ and bending curvature κ , are contained within the nondimensional formulation.

In this article, we focus on the planar case and therefore the simulation model becomes simpler. The twisting force does not need to be taken into consideration and the z -coordinate of the nodes can be ignored. As such, our simulation model has $2N$ degrees of freedom for N nodes. Since bending deformation is energetically cheaper in rods compared with stretching strain, the rod can be considered inextensible. The forward process can be represented with $\Gamma_0(\mathbf{x}, \mathbf{y}) \in \mathbb{R}^2 \rightarrow \Gamma(\mathbf{x}, \mathbf{y}) \in \mathbb{R}^2$, where \mathbf{x} and \mathbf{y} are N -sized vectors consisting of the x - and y -coordinates of the nodes, respectively.

The forward simulation makes the following four assumptions.

- (1) The first node \mathbf{X}_0 is fixed at $(0, 0)$.
- (2) The first edge $\mathbf{e}^0 = \mathbf{X}_1 - \mathbf{X}_0$ is fixed before and after deformation. This is analogous to clamped boundary condition. The other end of the rod is free. If the second order accurate scheme is required in other cases, this assumption can be modified referring to Reference 37.
- (3) Self-contact and friction force of the elastic rods are neglected during deformation.
- (4) The simulation process will stop and exit automatically if speed of the last node is smaller than a predefined threshold v_{th} , for example, 10^{-6} . This ensures that (1) no excessive time is consumed so that the real-time performance of our proposed method is maintained and (2) the simulation has run long enough for the rod to reach its static deformed shape. Only Checking the speed of the last node is enough to judge whether the simulation has been finished for the clamped-free models in this article.

Figure 1 shows the deformed shape Γ outputted from the DER model and the undeformed curve Γ_0 . The direction of gravity is along the negative y -axis. In this article, unless stated otherwise, the material and geometric parameters are: radius of rod $r_0 = 1$ mm (only circular cross-section rod is discussed in this article), density of rod $\rho = 1000$ kg/m³, gravitational acceleration $g = 9.8$ m/s², Young's modulus $E = 1.78 \times 10^7$ Pa. The nodes are distributed uniformly along the rod and the length of each edge is $\Delta l = 1$ cm. It should be noted that the ratio between the rod length and its radius is required to meet $L/r \geq 10$ in DER theory.^{30,38} Due to the nondimensionalization scheme described in the next Section, our results are not restricted to the specific values of these physical parameters.

In order to verify the convergence effect, a simple elastic rod is inputted into the forward model, as shown in Figure 2, under three configurations: $l_{gb} = 0.11, 0.23, 0.50$ m corresponding to $E = 1 \times 10^8, 1 \times 10^9, 1 \times 10^{10}$ Pa if other parameters stay unchanged. The undeformed horizontal rod ($L = 0.6$ m) deforms and produces three shapes in Figure 2A. According to Euler's theory of the elastica, as the rod vertex number N increases, the solution provided by the discrete elastic rod formulation converges to the deformed centerline.³⁰ Six edge lengths are adopted with $\Delta l = [0.02, 0.015, 0.01, 0.008, 0.005, 0.002]$ m, and thus, the rod vertex number is $N = [31, 41, 61, 76, 121, 301]$ respectively. The last vertex of the deformed rods are plotted in Figure 2B, showing that excellent agreement is achieved for the deformed rods when different discretization parameter is adopted. Relative vertical deviation of the last vertices for deformed rods between $N = 31, 41, 61, 76, 121$ and $N = 301$ can be calculated according to $\Delta d/d = \|(\mathbf{y} - \mathbf{y}_{N=301})/\mathbf{y}_{N=301}\|$. It can be found from Figure 2C that as N increases, relative deviation of the last node for elastic rods become smaller in y -direction after deformation. Even for the sparsest case, that is, $N = 31$ or $\Delta l = 0.02$ m, the maximal vertical deviation is less than 0.06. Although more vertex or shorter edge length could lead to a more accurate result, much more computation time is

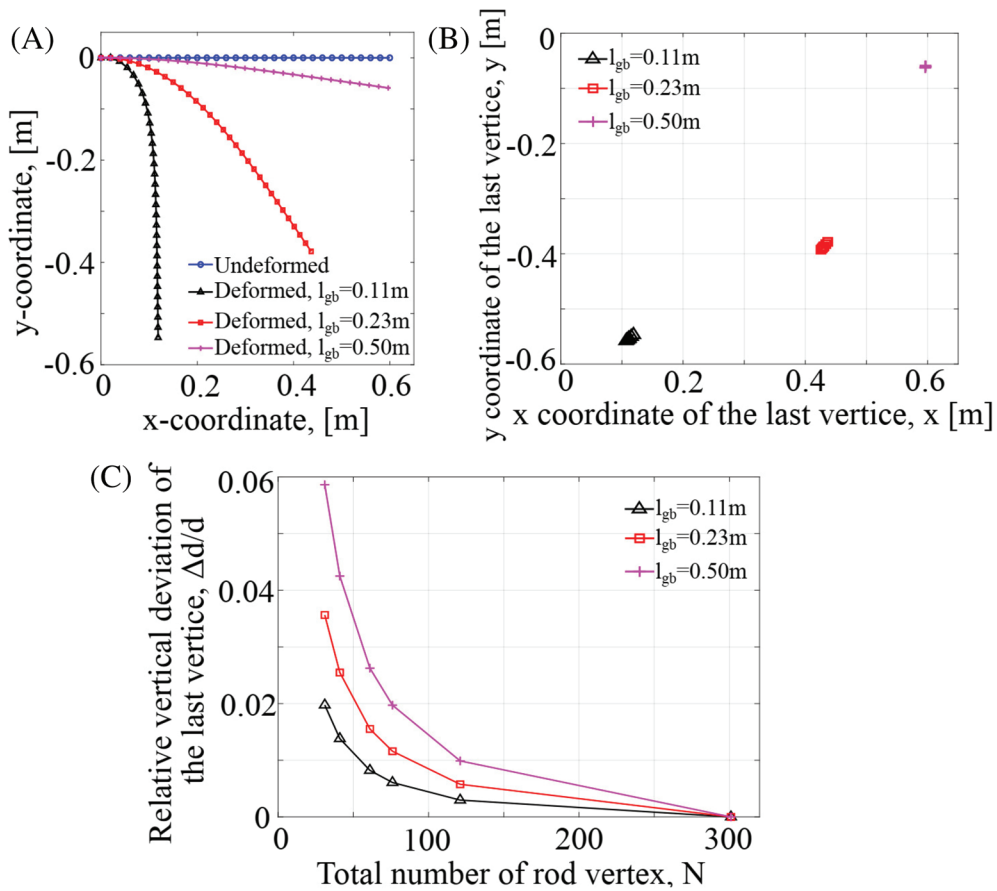


FIGURE 2 Convergence validation of the forward model. (A) Undeformed and deformed rods with different l_{gb} . (B) Distribution of the last vertices when the total number of rod vertex is [31, 41, 61, 76, 121, 301]. (C) Relative deviation of the last node for different rod vertex numbers

required and therefore the real-time performance will be degraded. In this article, Δl is chosen as 1 cm which could be easily changed in the future to meet the designers' demands.

2.2 | Inverse process

It has been proved that there exists an unique original shape for a deformed curve under gravity.²⁷ The inverse problem of interest in this article is how to find out the undeformed shape when the deformed curve and relevant material parameters are given. In planar case, the centerline of an elastic rod can be represented by a series of angles $\theta = [\theta_0, \theta_1, \dots, \theta_{N-2}]$, that is, orientations of all edges, as each edge shares the same length Δl and the rod is almost inextensible.

In addition to the geometry (θ), the material parameters of the rod and magnitude of gravitational pull also affect the deformation process. Fortunately, we can employ one nondimensional governing parameter to encapsulate the effect of these material and gravity parameters. First, a length-scale—also known as the gravito-bending parameter, L_{gb} —arises from the competition between bending and gravity such that.³⁶

$$L_{gb} = \left(\frac{r_0^2 E}{8 \rho g} \right)^{1/3}. \quad (5)$$

If we normalize the discretization parameter Δl , then the deformation process depends only on $\frac{\Delta l}{L_{gb}}$ and the orientation angles. Therefore, instead of listing all the material and gravity parameters, we only need to specify $\frac{\Delta l}{L_{gb}}$. Instead of

representing the deformation process as $\Gamma_0(\mathbf{x}, \mathbf{y}) \rightarrow \Gamma(\mathbf{x}, \mathbf{y})$, it is convenient to use $\Gamma_0\left(\theta^0, \frac{\Delta l}{L_{gb}}\right) \rightarrow \Gamma\left(\theta, \frac{\Delta l}{L_{gb}}\right)$, where θ^0 and θ are the sets of orientation angles in undeformed and deformed configurations. Simple trigonometry is needed to reconstruct \mathbf{x} and \mathbf{y} from the sequence of orientation angles. As will be discussed in more detail in Section 3.2, the orientation angles are related to the curvature of the centerline of the rod. The inverse problem now boils down to the optimization problem given below.

$$\begin{aligned} & \text{Given } \Gamma\left(\theta, \frac{\Delta l}{L_{gb}}\right) \in \mathbb{R}^2, \\ & \text{find } \Gamma_0\left(\theta^0, \frac{\Delta l}{L_{gb}}\right) \\ & \text{that minimizes } e = \left\| \Gamma\left(\theta, \frac{\Delta l}{L_{gb}}\right) - \hat{\Gamma}\left(\theta, \frac{\Delta l}{L_{gb}}\right) \right\|, \\ & \text{subject to} \\ & \hat{\Gamma}\left(\theta, \frac{\Delta l}{L_{gb}}\right) = f\left(\Gamma_0\left(\theta^0, \frac{\Delta l}{L_{gb}}\right)\right), \end{aligned} \quad (6)$$

where the last equation represents that the shape $\hat{\Gamma}$ is a function of the undeformed shape Γ_0 and can be evaluated using DER. Since $\frac{\Delta l}{L_{gb}}$ does not vary with deformation, only θ^0 is the unknown variable. The error, e , between the target and the designed deformed curve is

$$e = \frac{1}{N \cdot L} \sum_{i=1}^N \sqrt{(x_i - \hat{x}_i)^2 + (y_i - \hat{y}_i)^2}, \quad (7)$$

where N is the total number of vertices, \hat{x}_i and \hat{y}_i are the x - and y -coordinates of the i th node on the designed deformed curve, respectively, \hat{x} and \hat{y} are the coordinates on the given deformed curve, and $L = (N - 1)\Delta l$ is the whole length of the elastic rod.

3 | METHOD

In this section, we outline the algorithm to solve for the undeformed shape given the deformed shape. The main idea behind the method is deceivingly simple: solve for the bending curvature (related to the difference between two consecutive orientation angles) at each node one at a time, starting from the free end and ending at the clamped end.

3.1 | Relationship between deviations and unknown variables

Two issues make the problem of interest in this article more challenging: (1) Each orientation angle interplays with other angles and all of them has to be achieved accurately. Large deviation may occur if only one angle is not precise enough even though all the other angles are accurately predicted. (2) The total deviation e does not decrease monotonically as the number of unknown variables, that is, orientation angles of the undeformed curve, is reduced.

In order to explain it, three sample curves including the one given in Figure 1 are chosen and shown in Figure 3A1–C1. The corresponding orientation angles are shown in (A2), (B2), and (C2). First, $N - 2$ angles are generated in random to constitute an initial guess for the undeformed shape with the turning angle between each two consecutive edges falling into the range $[-\pi/5, \pi/5]$. This bound is used to generate a smooth curve without any unphysical sharp cusp along the rod. It should be noted that the first orientation angle is fixed before and after deformation with assumption (2) and therefore it is a priori information. Then the first n ($N \leq n \leq N - 2$) values among the initial guessed angles are replaced by the corresponding true undeformed angles, where $n = 0, 2, \dots, N - 2$. With each replacement (i.e., increasing n), the deviation e is calculated and thus $N - 1$ errors are obtained. Specially, $n = 0$ refers to the error for the initial guess and $e = 0$ when $n = N - 2$ meaning all the unknown variables have been replaced by true values. The errors are shown in Figure 3A3–C3;

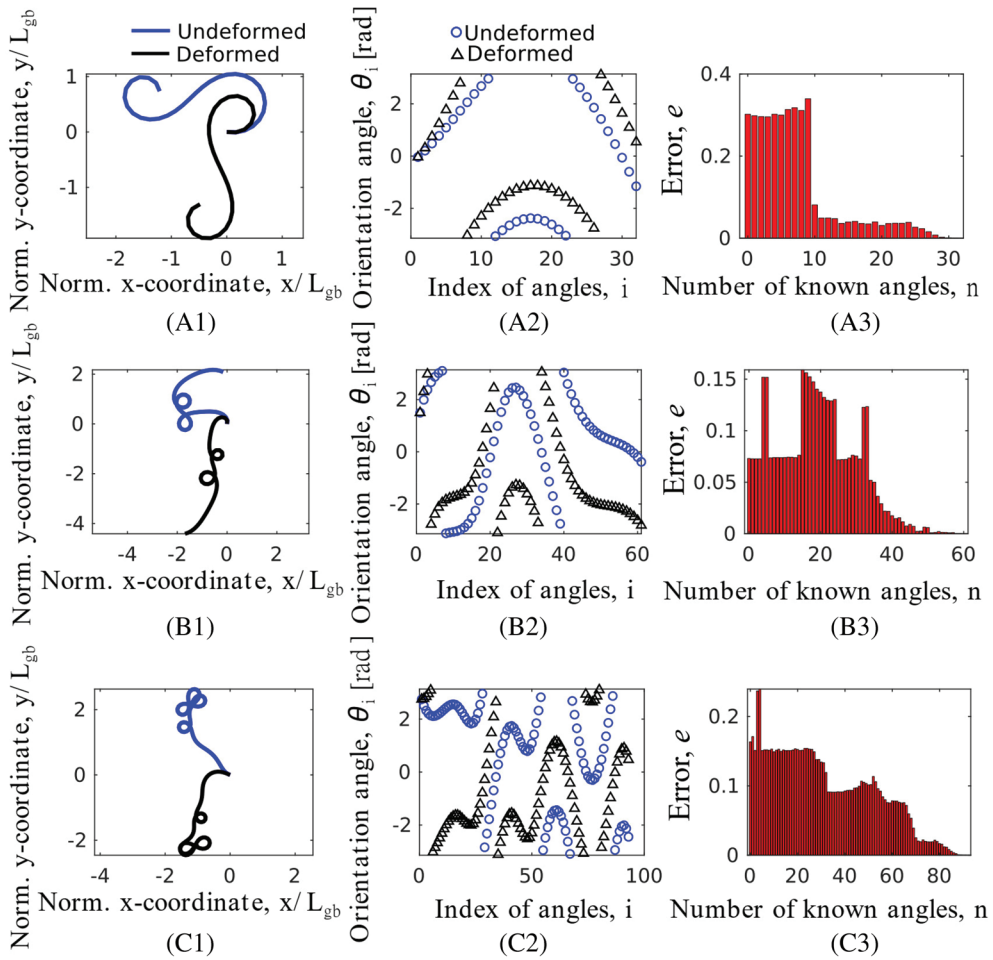


FIGURE 3 Three sample curves to show the variation of errors with respect to the decreased number of unknown variables. (A1), (B1), and (C1) show the three undeformed and deformed curves, and their orientation angles are given in (A2), (B2), and (C2) respectively. (A3), (B3), and (C3) show the error variation when the first n variables are replaced by true values. In the three cases, the total number of vertices N are 33, 62, and 94 while the parameter $\Delta l/L_{gb}$ are 0.1639, 0.1427, and 0.0799

it is obvious that the deviation does not change monotonically as the number of unknown variables decreases. This makes traditional optimization algorithms prone to getting stuck in local minimum.

3.2 | Bottom-up design method

Considering that multivariate optimization in parallel is prone to getting stuck in local minimum, finding the optimal variables one by one in sequence—whenever possible—is often a more robust option. In this problem, mechanical analysis (refer to Figure 4) provides an insight that we use to solve the problem one variable at a time. A whole curve in Figure 4A can be decomposed into two parts as shown in Figure 4B. Assuming the external force is gravity, the force and moment applied to the last edge of part I by part II can be calculated from

$$\mathbf{F} = \sum_{j=N_1-1}^{N-2} \Delta m_j g, \quad (8)$$

$$\mathbf{M} = \sum_{j=N_1-1}^{N-2} \mathbf{r}_j \times \mathbf{F}_j, \quad (9)$$

where Δm_j is the mass of the j th edge that can be easily calculated from the density, the edge length, and the cross-sectional area of the rod. There are a total of N nodes on the whole rod and N_1 and N_2 nodes on part I and part II, respectively.

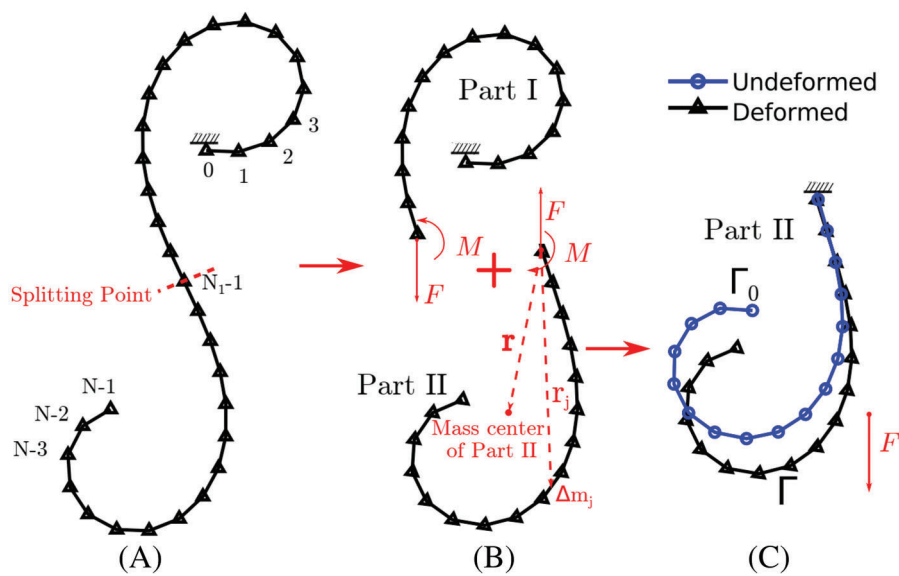


FIGURE 4 Equivalent decomposition of a whole elastic rod. (A) could be decomposed into two parts as shown in (B). Part II and its undeformed shape are given in (C) as its first edge is fixed

As such, $N_1 + N_2 = N + 1$ as both of the parts $(N_1 - 1)$ th node, that is, the splitting point shown in Figure 4. The position vector from the splitting point to the mass center of the j th edge is r_j . We can now simply delete one of the parts and replace it with the force and moment on the other part from Equations (8) and (9).

Here we define an elastic rod in stable state meaning that it can always stay in its deformed shape even if its free end is dragged to different directions and then relaxed. In essence the deformation process is the transformation of internal elastic energy to gravitational energy. Derouet-Jourdan et al.²⁰ proposed a sufficient but not necessary condition to estimate if an elastic rod is stable; this condition is

$$\frac{EI}{\rho S} > \lambda, \quad (10)$$

where S is the cross-sectional area of the rod and λ is an inherent parameter, which is only related to the deformed curve shape. If an elastic rod cannot maintain stability, increasing EI or decreasing ρS can help it reach a stable state.

Let us consider the deformation of part II in Figure 4C. The whole undeformed rod is first split into part I and part II; then part II of the undeformed rod is rotated so that its first edge is aligned to the first edge of the part II of the deformed rod. If this undeformed portion deforms under gravity (first two nodes are fixed), it will assume the same deformed shape as the portion on the whole deformed curve (Figure 4C). The clamped boundary exerts a force and a moment on the rod and this force and moment are equal to the ones exerted by part I on part II. In other words, we can split smaller segments of the rod from the free end and the solution to the smaller problem constitutes part of the solution to the larger problem.

Exploiting this idea, a bottom-up design method is proposed and the procedure is shown in Figure 5. In a case where the whole rod consists of N nodes, what should be solved is the $N - 2$ optimal turning angles $\Delta\hat{\theta}^0$ which is defined as

$$\Delta\hat{\theta}_{i-1}^0 = \hat{\theta}_i^0 - \hat{\theta}_{i-1}^0, i = 1, 2, \dots, N - 1, \quad (11)$$

where $\Delta\hat{\theta}_i^0$ is the (i) th element of the vector $\Delta\hat{\theta}^0$. This turning angle is directly related to the bending curvature at the i th node, κ_i , through the following relation,³⁰

$$\kappa_i = \frac{2 \tan \frac{\Delta\theta_i}{2}}{\Delta l}. \quad (12)$$

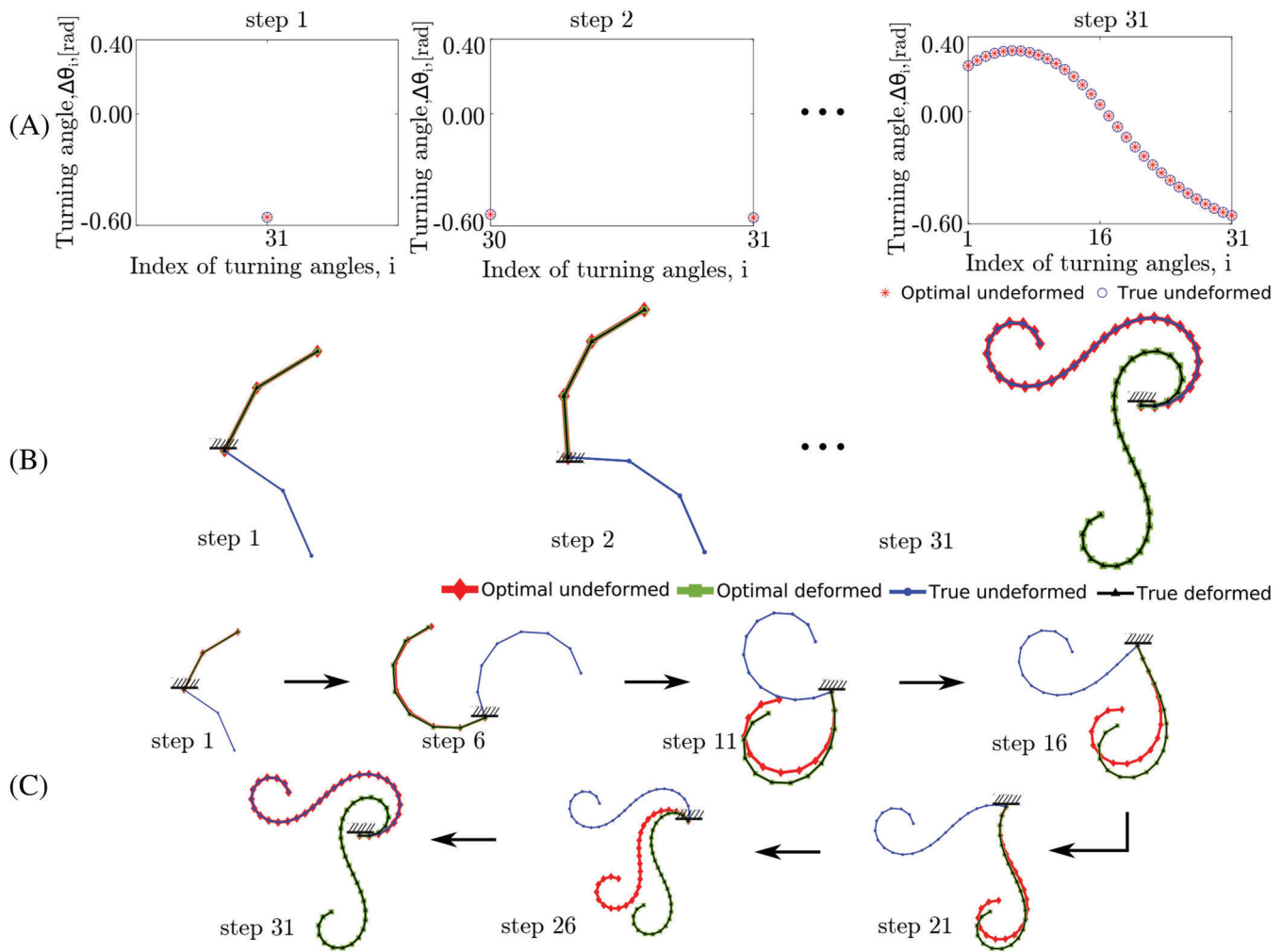


FIGURE 5 Principle of the bottom-up design method. Turning angles and the curve at step 1, step 2, and step 31 are given in (A) and (B). Seven intermediate steps are listed in (C) to illustrate the procedures. $\Delta l/L_{gb} = 0.1639$. “True undeformed” curve is the undeformed configuration and “true deformed” is the deformed shape under gravity obtained from DER. “Optimal undeformed” is the shape computed from the proposed algorithm, given the true deformed curve. “Optimal deformed” is the output (deformed shape under gravity) of DER given the optimal undeformed shape

Figure 5 presents an example with $N = 33$ nodes on the rod. At first, a curve consisting of the last two edges is regarded as the target deformed curve to design. The algorithm searches for the optimal turning angle $\hat{\theta}_{N-2}^0$. In combination with the orientation angle θ_{N-2} of edge e^{N-2} , the orientation angle sequence and the temporary optimal undeformed curve $\hat{F}_0^{N_e=2}(x, y)$ is obtained, in which N_e indicates the number of edges. Secondly, the algorithm searches for the optimal turning angle $\hat{\theta}_{N-3}^0$. In combination with θ_{N-3} and $\hat{\theta}_{N-2}^0$ that is found in the previous step, the temporary optimal undeformed curve $\hat{F}_0^{N_e=3}(x, y)$ is obtained. This process is repeated until the first turning angle $\hat{\theta}_0^0$ is found and $\hat{F}_0^{N_e=N-1}(x, y)$ is obtained. Therein for any intermediate curve, its orientation angle $\hat{\theta}_{i-1}$ can be calculated using

$$\hat{\theta}_{i-1}^0 = \theta_0 + \sum_{j=1}^{i-2} \Delta\hat{\theta}_j^0. \quad (13)$$

In Figure 5A, it can be found at every step, the searched optimal turning angles agree excellently with the true target values. The temporary optimal undeformed rod only differs from the true undeformed one with a scalar rotation angle (i.e., rigid body rotation) before the final step and after deformation it agrees perfectly with the true deformed shape.

Algorithm 1. The proposed optimized searching algorithm

Inputs:

- $\Delta\theta_{\min}, \Delta\theta_{\max}$ \triangleright minimal and maximal limit of the variables.
- $\Gamma(x, y)$ \triangleright target deformed curve with N nodes.
- $e_{\text{tol}}, \text{iter}_{\text{lim}}$ \triangleright maximal tolerance of error and maximal iteration number.
- lb, ub, k_r \triangleright lower and upper boundary and searching range factor.
- N_{seed} \triangleright number of seeds in the current range.

- 1) Generate $\Delta\theta_{N-2}^0$ within $[\Delta\theta_{\min}, \Delta\theta_{\max}]$ in random
- 2) Transform it to curve $\hat{\Gamma}_0^{N_e=2}(x, y)$
- 3) Use DER to calculate e for $\hat{\Gamma}_0^{N_e=2}(x, y)$ via Equation~(7): $\mathbf{e}(0) \leftarrow e$ $\triangleright \mathbf{e}$ is a vector that will store the errors associated with different solutions
- 4) $lb \leftarrow \Delta\theta_{\min}, ub \leftarrow \Delta\theta_{\max}, \text{iter} \leftarrow 1$
- 5)

while $e > e_{\text{tol}}$ and $\text{iter} \leq \text{iter}_{\text{lim}}$ **do**

- for** $i = 1:N_{\text{seed}}$ **do**
 - $\Delta\theta_{N-2}^0(i) \leftarrow \Delta\theta_{\min} + (i - 1) \cdot (\Delta\theta_{\max} - \Delta\theta_{\min}) / (N_{\text{seed}} - 1)$ $\triangleright \Delta\theta_{N-2}^0$ is N_{seed} -sized vector and $\Delta\theta_{N-2}^0(i)$ is its i -th element
 - Calculate $\mathbf{e}(i)$ following 2)~3).
- end for**
- $\mathbf{e} = [\mathbf{e}(0), \mathbf{e}(1), \dots, \mathbf{e}(N_{\text{seed}})]$
- $\mathbf{e}_{\text{sorted}} = \text{sort}(\mathbf{e})$ \triangleright Sort \mathbf{e} in ascending order to get $\mathbf{e}_{\text{sorted}}$
- $\Delta\theta_{\text{sorted}}$ is a sorted version of $\Delta\theta_{N-2}^0$ based on $\mathbf{e}_{\text{sorted}}$
- $\Delta\theta_{lb} \leftarrow \min([\Delta\theta_{\text{sorted}}(1), \Delta\theta_{\text{sorted}}(2)])$
- $\Delta\theta_{ub} \leftarrow \max([\Delta\theta_{\text{sorted}}(1), \Delta\theta_{\text{sorted}}(2)])$
- if** $\Delta\theta_{ub} - \Delta\theta_{lb} > 0$ $\&$ $[\Delta\theta_{lb}, \Delta\theta_{ub}]$ differs from last iteration **then**
 - $\Delta\theta_{\min} \leftarrow \max([\Delta\theta_{lb} - (\Delta\theta_{ub} - \Delta\theta_{lb}) \cdot k_r, lb])$
 - $\Delta\theta_{\max} \leftarrow \min([\Delta\theta_{ub} + (\Delta\theta_{ub} - \Delta\theta_{lb}) \cdot k_r, ub])$
- else**
 - break
- end if**
- $\text{iter} = \text{iter} + 1$

end while

- 6) $\Delta\hat{\theta}_{N-2}^0 = \Delta\theta_{\text{sorted}}(1)$ \triangleright Optimal turning angle
- 7) Based on $\Delta\hat{\theta}_{N-2}^0$, search for the optimal turning angle $\Delta\hat{\theta}_{N-3}^0$ following 1)~6) and $N_e = 3$. Repeat until all optimal turning angles are found.

3.3 | Optimized searching algorithm

In previous Section 3.2, one turning angle of the optimal undeformed curve would be searched at every step. The optimized searching algorithm is presented in Algorithm 1. It starts with a random guess of the turning angle to be solved in procedure (1), whose upper and lower boundary is preset by the user. Then, the guessed curve could be obtained by transforming the known angles to a $x - y$ curve $\hat{\Gamma}_0^{N_e=2}(x, y)$, which is passed to the DER model to output the deformed curve and calculate the defined error, e , as depicted in procedure (2) and (3). In the first iteration loop, the lower and upper boundary equal to the minimal and maximal turning angle provided by the user and the iteration loop number starts from 1. In procedure (5), the searching range of the optimized turning angle is first split in uniform and then shrunk gradually according to the errors between the target shape and the deformed curve from the guessed undeformed shape. There exist N_{seed} errors after the calculation and the error vector is sorted to locate the region where the optimized turning angle may appear. A finer searching range will be found out iteration-by-iteration while both the minimal error is larger than the preset error tolerance and the iteration loop number is less than the preset iteration limit. The searched optimized turning angle $\Delta\hat{\theta}_{N-2}^0$ is $\Delta\theta_{\text{sorted}}(1)$ corresponding to the value that achieves the minimum error compared with

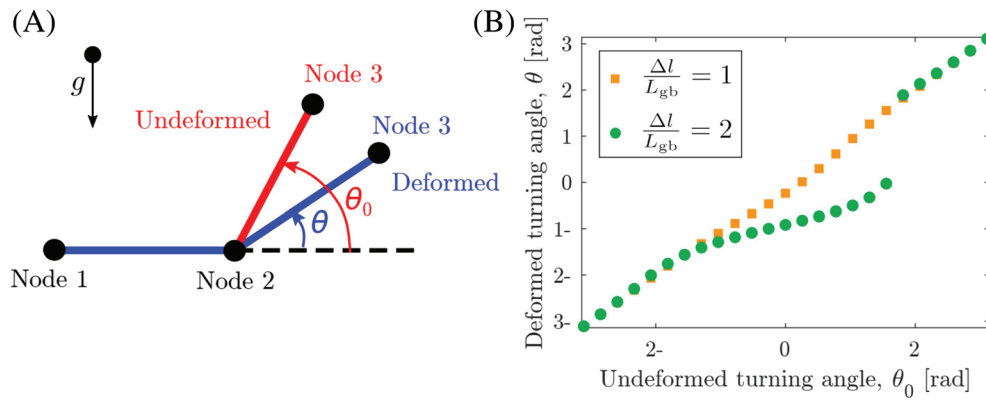


FIGURE 6 Illustration of existence of inverse solution for 3-node rod. (A) The undeformed and deformed rod. (B) Correspondence between the undeformed and deformed turning angle of edge 2, e^1 , in (A). Different relationships can be found in cases of $\Delta l/L_{gb} = 0.1$ and $\Delta l/L_{gb} = 10$

the target design (procedure 6). After the optimized value of the last turning angle is obtained, the searching algorithm continues following the above procedures to search for the last second turning angle until all the optimal values are found.

In general, the searching range will be split and shrunk iteration-by-iteration, during which, the optimal variable that achieves the smallest error e in last iteration will be passed to the next iteration. Parameter N_{seed} is the number of seeds used to split the current range, which controls the precision of the final solution as well as the searching speed. Another parameter k_r is set to configure how large the searching range will be in next iteration, which should range within $[0, 1]$. In this article, $N_{seed} = 30$ and $k_r = 0.5$.

It should be noted that the magnitude of errors has significant influence on the inverse solution since the total error will be magnified if a system comprises multiple variables containing inevitable errors.¹⁵ Although the bottom-up method that determines only one turning angle each time is a helpful strategy to control the total errors, the error produced at each time step with Algorithm 1 should remain tiny sufficiently at the same time. It can be realized by adjusting the user-specified parameter, e_{tol} , which is trade-off between the precision and the time cost of the predicted undeformed shape.

3.4 | Existence of inverse solutions

Before exploring the performance of the proposed method, it should be made clear first that not every target curve under any parameter configuration has an inverse solution. In Figure 6A, we take the simplest case with three nodes and two edges as an example to illustrate this concept. The first edge e^0 (i.e., Node 1 and Node 2) is fixed and the lumped mass on the third free node is $m = \frac{\Delta l}{2} \pi r_0^2 \rho$. Under gravitational force $F = mg$, the other edge e^1 deforms with the turning angle changing from its undeformed value of θ_0 to the deformed value of θ . As stretching and twisting energy are neglected in 2D case, the total energy can be formulated as Equation (14).

$$\begin{aligned} E &= E_b + E_g \\ &= \frac{1}{2\Delta l} EI(\kappa - \kappa_0)^2 + mg(\Delta l \sin \theta - \Delta l \sin \theta_0) \\ &= \frac{\pi r_0^2}{2} \left[\frac{Er_0^2}{\Delta l} \left(\tan \frac{\theta}{2} - \tan \frac{\theta_0}{2} \right)^2 + \Delta l^2 \rho g (\sin \theta - \sin \theta_0) \right]. \end{aligned} \quad (14)$$

Given the turning angle θ_0 of undeformed shape, we can find out θ via minimizing Equation (14).

$$\theta = \operatorname{argmin} E(\theta). \quad (15)$$

There is only one variable θ and it can thus be solved by solving the equation $\frac{dE}{d\theta} = 0$, that is, finding the solution of Equation (16).

$$\begin{aligned} & \left(\tan \frac{\theta}{2} \right)^5 - K_2 \left(\tan \frac{\theta}{2} \right)^4 + 2 \left(\tan \frac{\theta}{2} \right)^3 \\ & - (K_1 + 2K_2) \left(\tan \frac{\theta}{2} \right)^2 + \tan \frac{\theta}{2} - (K_2 - K_1) = 0, \end{aligned} \quad (16)$$

where $K_1 = \frac{\Delta l^3 \rho g}{E r_0^2} = 8 \left(\frac{\Delta l}{L_{gb}} \right)^3$ and $K_2 = \tan \frac{\theta_0}{2}$. Note that θ only depends on θ_0 and $\frac{\Delta l}{L_{gb}}$. In Figure 6B, the deformed angle, θ , is presented as a function of undeformed angle, θ_0 , at two values of $\frac{\Delta l}{L_{gb}} = 1.0, 2.0$. In case of $\frac{\Delta l}{L_{gb}} = 1$, the rod is stiff enough to withstand gravity and $\theta \approx \theta_0$. On the other hand, if $\frac{\Delta l}{L_{gb}} = 2$ and the rod is “soft”, the relation between the undeformed and deformed angles are nonlinear. Interestingly, when the deformed angle, θ , is approximately between 0 and $\pi/2$, there is no corresponding undeformed angle. Physically, this means that the rod is too soft and it is unable to supply adequate elastic energy to maintain a deformed shape with $0 \lesssim \theta \lesssim \pi/2$.

4 | RESULT AND DISCUSSION

4.1 | Validation of natural curves

In general case, the curves used for validation should be smooth to mimic natural elastic rods. Since the x - and y - coordinates of the nodes and the orientation angles change continuously along the arc length of a natural rod, we generate several random turning angles within $[-\pi/5, \pi/5]$ and then interpolate to produce smooth angle sequence and $x - y$ values. Spline interpolation is adopted in this article.³⁹ To characterize the effects of different material, geometry and external force, $\Delta l/L_{gb}$ ranges from 2×10^{-2} to 2×10^{-1} . If other parameters are kept unchanged, it is equivalent to change Young's Modulus from 1×10^{10} to 1×10^7 Pa. When $\Delta l/L_{gb} \rightarrow 0$, the deformation is negligible and the undeformed and deformed curves are the same. On the other hand, $\Delta l/L_{gb} \rightarrow \infty$, the deformed curve is a straight line along the direction of gravity, regardless of the undeformed shape.

The generated curves are regarded as undeformed curves and then inputted into the DER model to output the true deformed shape—the input to the proposed algorithm. With both undeformed and deformed curves at hand, the bottom-up design method is applied to find out the optimal original rods and compared with the true undeformed curves. Four generated curves of different lengths and $\Delta l/L_{gb}$ are presented in Figure 7. With the bottom-up design method, the optimal turning angle sequences are obtained as shown in Figures 7A1–D1. Excellent agreement between the optimal and true turning angles are found. After they are inputted into the simulation model, it is found as expected that the deformed shapes of the optimal rods agree with the true deformed shape. Effect of $\Delta l/L_{gb}$ is also obvious—a smaller value of $\Delta l/L_{gb}$ (i.e., large L_{gb}) results in less deformation.

4.2 | Inverse design of special curves

In this section, four special curves are designed as the target deformed rods. The bottom-up design method is applied to find out the optimal undeformed shape. As the true undeformed curve is unknown, the found optimal curve will be inputted into the simulation model and the deformed rod is compared with the target curve. Mathematical formulations for the four target rods are given below.

$$\begin{cases} x = A \cdot e^{t(s)/w} \cdot \sin(w \cdot t(s)) \\ y = -\lambda \cdot t(s) \end{cases}, \quad (17)$$

$$\begin{cases} x^2(s) + (y(s) + R_1)^2 = R_1^2, s \in [0, 0.32] \\ x^2(s) + (y(s) + 3R_1)^2 = R_1^2, s \in (0.32, 0.64] \end{cases}, \quad (18)$$

$$y(s) = ax^2(s) + bx(s), \quad (19)$$

$$\begin{cases} (x(s) + c_1)^2 + (y(s) + c_2)^2 = R_2^2, s \in [0, 0.35] \\ \begin{cases} x(s) = (h_1 + h_2\theta(s)) \cdot \cos(\theta(s)) + k_1 & s \in (0.35, 1] \\ y(s) = (h_1 + h_2\theta(s)) \cdot \sin(\theta(s)) + k_2 \end{cases} \end{cases}, \quad (20)$$

where s is the arc length, $t(s)$ and $\theta(s)$ are functions of s , and the x - and y -coordinates of the centerline are functions of s . A discrete rod is inputted to DER with edges of the same length. Relevant parameters can be found in Table 1.

As shown in Figure 8A2, curve I is a conical sine curve with a length of $71L_{gb}$. Turning angles for the optimal undeformed shape are shown in Figure 8A1, whose variation resembles a zigzag wave of increasing amplitude. Some deviation between the target rod and the optimal deformed curve is found near the free end—this is qualitatively related to the low stiffness of the material (see Equation (10)). A smaller $\Delta l/L_{gb}$ by increasing the Young's Modulus, E (or increasing the radius of rod, r_0 , or reducing density, ρ) will help improve the agreement. This will be discussed in more detail in Figure 9). In Figure 8B, two semicircles of the same radius are connected as the target rod. A jump from negative to positive value can be found in Figure 8B1 in the turning angle sequence of the optimal undeformed curve, indicating the abrupt turning of arc direction. Target shape III in Figure 8C is a parabolic curve with one end fixed at the origin point. The fourth elastic rod in Figure 8D is constructed by a part of arc and another part of Archimedean spiral in order to mimic the shape of tendrils in natural world.

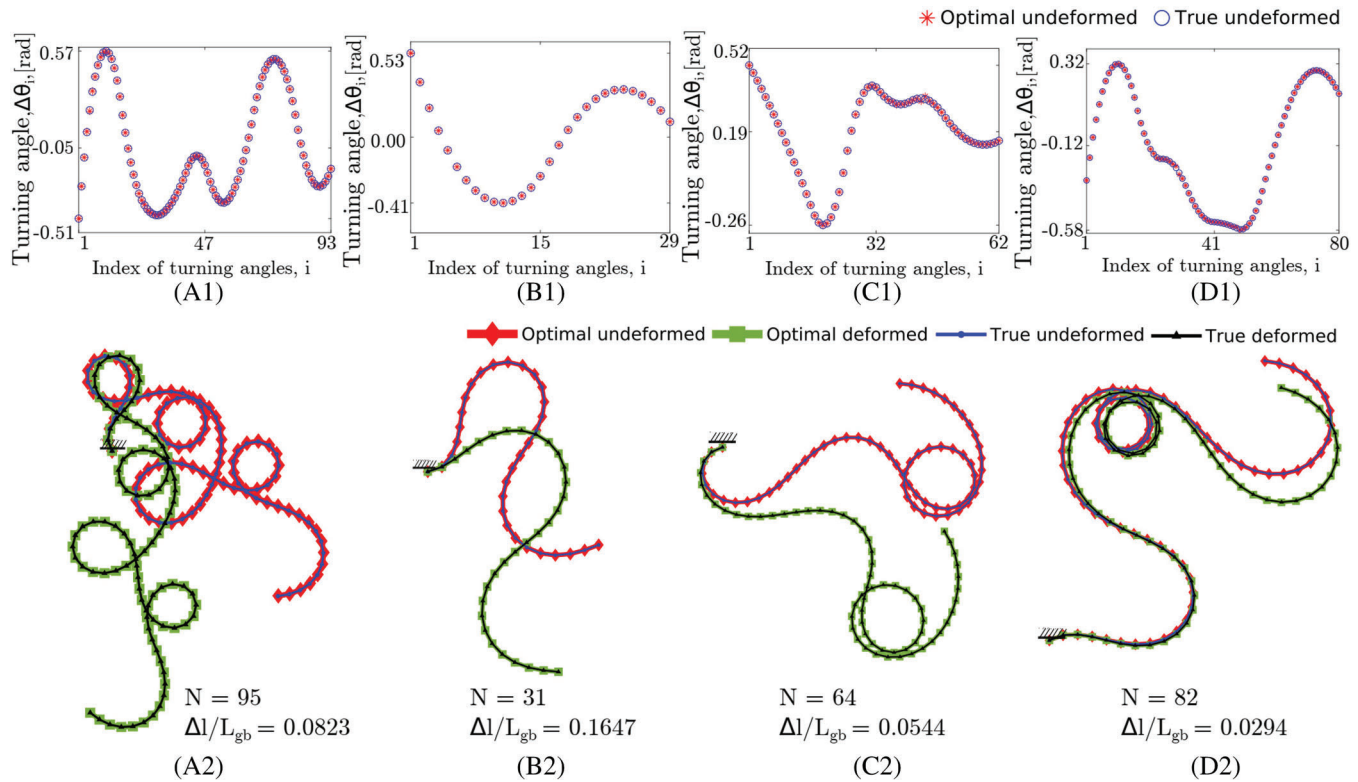


FIGURE 7 Four curves generated in random to validate the effect of the bottom-up design method. (A1), (B1), (C1), and (D1) show the turning angles while their corresponding curves are given in (A2), (B2), (C2), and (D2). The number of vertices N and parameter $\Delta l/L_{gb}$ of each curve are indicated below

TABLE 1 Parameters in Equation (17)~(20)

A	w	λ	R₁	a	b	c₁
0.015	3	0.08	0.1	16	-3	0.249
c_2	R_2	h_1	h_2	k_1	k_2	
0.016	0.25	0.006	0.008	-0.249	0.126	

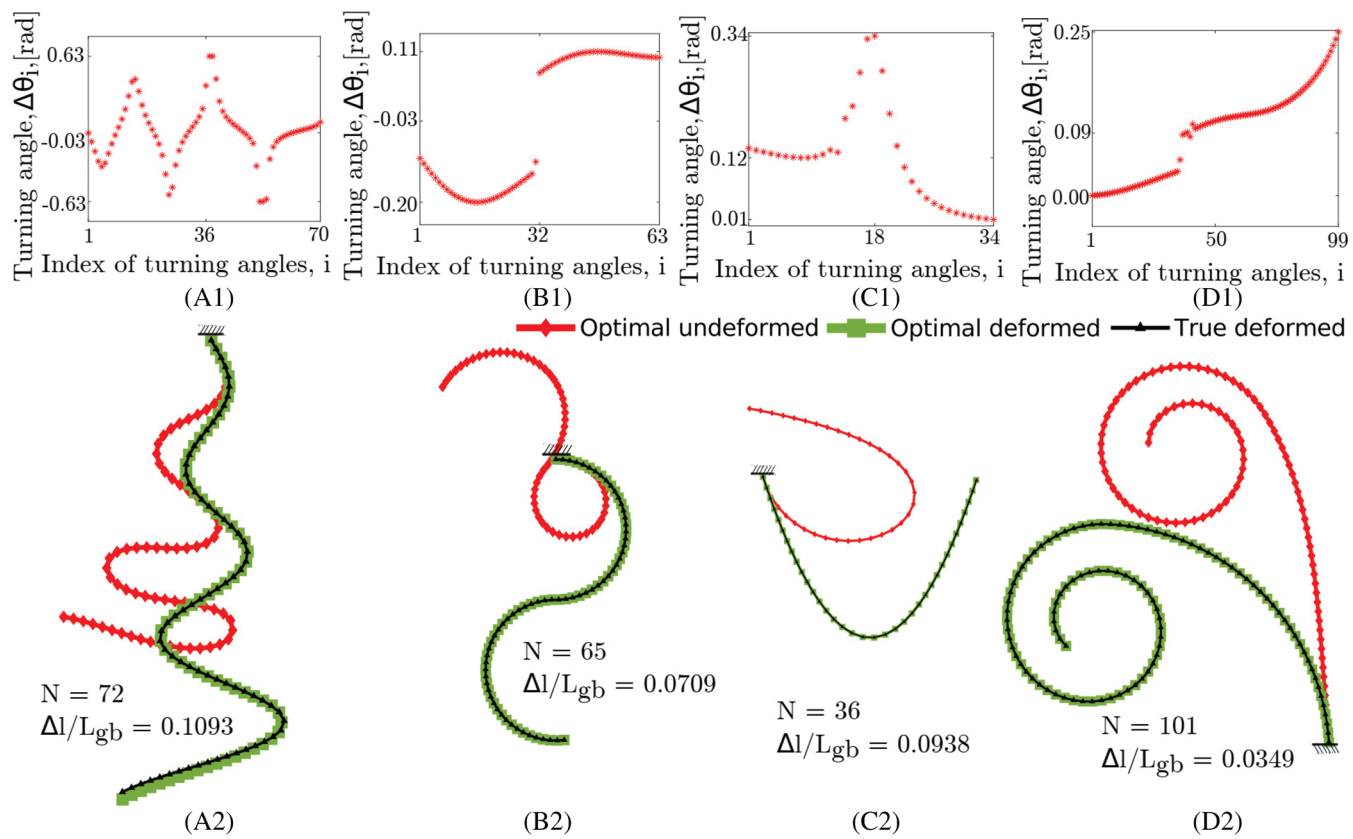


FIGURE 8 Undeformed shapes found by the bottom-up design method for four constructed special curves: I. conical sine wave, II, connected semicircles, III, parabolic curve, IV, tendril shape (arc+Archimedean spiral). (A1), (B1), (C1), and (D1) show the turning angles while their corresponding curves are given in (A2), (B2), (C2), and (D2). The number of vertices N and parameter $\Delta l/L_{gb}$ of each curve are indicated below. See the deformation process in [Movie S1](#)

Geometrical and material parameters as well as external forces usually impact the inverse design result.^{27,40,41} In order to explore their effects in Figure 9, different values of $\Delta l/L_{gb}$ are utilized in the case of Curve IV, tendril. By changing Young's Modulus ranging from $E_{\min} = 5 \times 10^7$ Pa to $E_{\max} = 5 \times 10^9$ Pa with a uniform interval in the logarithmic space given in Equation (21), seven $\Delta l/L_{gb}$ are produced within $[0.0250, 0.1162]$ in Figure 9A1–A7 to inversely design a tendril rod.

$$E_i = 10^{\log_{10} E_{\min} + (\log_{10} E_{\max} - \log_{10} E_{\min}) \cdot (i-1)/(N_Y-1)}, \quad (21)$$

where N_Y is the total number of Young's Modulus values and $i = 1, 2, \dots, N_Y$. It indicates that the nondimensional parameter, $\Delta l/L_{gb}$, plays a significant role in designing an elastic rod with given target shape. It may fail if an elastic rod of large $\Delta l/L_{gb}$ is used. In this case, changing the relevant parameters to reduce the value of $\Delta l/L_{gb}$ will be helpful. In the example, a good agreement is found when $\Delta l/L_{gb}$ is less than 0.0418 as their indicated errors is about 5×10^{-5} (Figure 9B). The shape of the undeformed rod varies with the Young's modulus; however, they will deform and agree excellently with the target shape once a small enough $\Delta l/L_{gb}$ is used. As an extreme case, the elastic rod will stay the same before and after deformation if $\Delta l/L_{gb}$ is too small.

4.3 | Pros and cons of the proposed method

In addition to the proposed method, there exist a variety of algorithms that may be optional for the search of an optimal solution, such as simulated annealing (SA), genetic algorithm (GA), and particle swarm optimization (PSO). These optimization algorithms are widely used as a heuristic search tool, especially in solving multivariable optimization

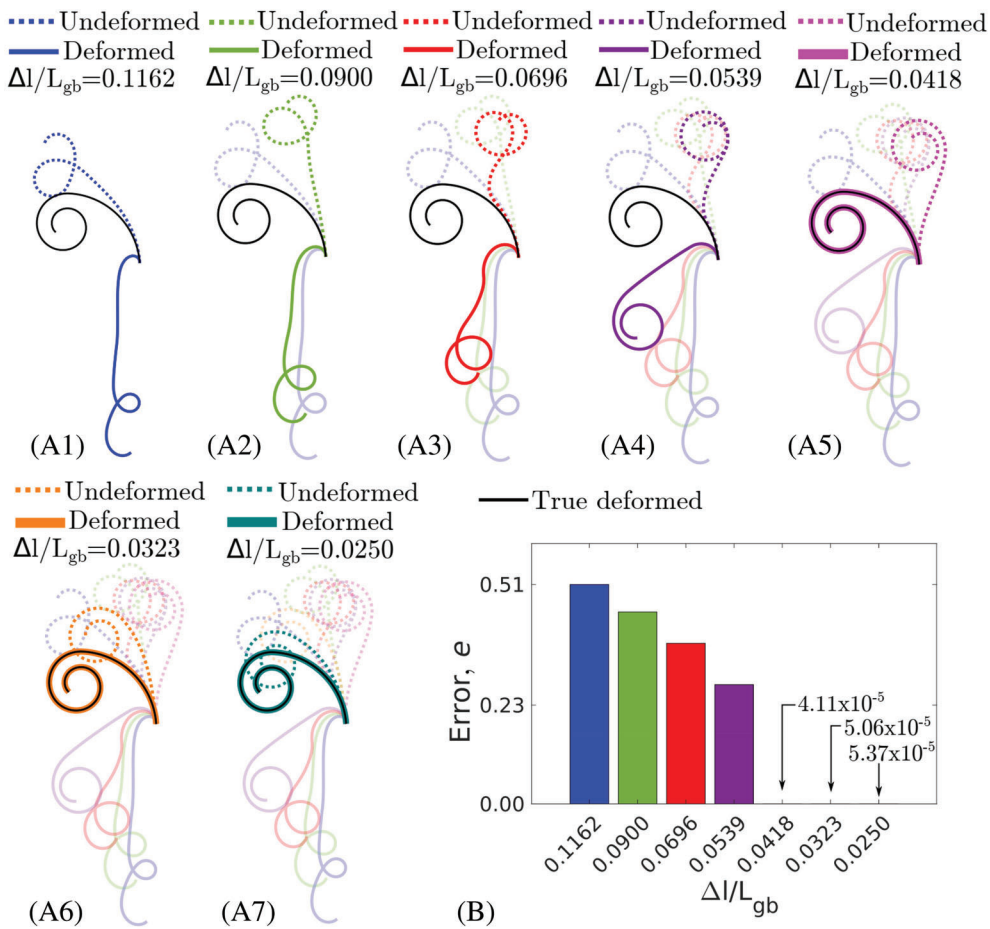


FIGURE 9 Result of tendril rod predicted with the proposed bottom-up design method for different $\Delta l/L_{gb}$, decreasing from 0.1162 to 0.0250, in (A1)~(A7). Their errors from the true target rod are shown in (B)

problems. Compared with the proposed optimization algorithm in this article, they can usually succeed in finding the optimal solution regardless of the mechanism underlying the problem to be solved, and therefore, are found easy to use. In the particular situation that the fitness function decreases monotonically with the number of unknown variables, these algorithms perform excellent even though the distribution and tendency of parameters to be solved are in random. However, it's not the case for the problem in this article, as Figure 3 reveals that variation of the error is not monotonic, where those optimization algorithms may be trapped at a local minimum and fail to find out the optimal solution. The proposed method, although proving successful in this article, cannot be applied to the other optimization processes directly if the underlying mechanism is totally different.

4.4 | Limitations

Although the inverse design of a target rod can be solved with the proposed bottom-up optimization method, it cannot be ensured that all the undeformed curves can be manufactured due to self penetration. For example, the original shape in Figure 7A2,C2,D2 is hard to experimentally fabricate since the loops result in a part of the rod penetrating other parts. In this case, the proposed method provides an insight that the target rod cannot be designed with current parameter configuration. Trying different material or changing other relevant parameters to decrease the value of $\Delta l/L_{gb}$ can help obtain the designed rods.

The scope of this article is limited to 2D case and therefore relatively simpler mechanical model is involved in developing the DER-based simulation tool. Twisting force and moment are not considered. In 3D case, twist angles will need to be taken into consideration when the bottom-up design method is constructed.

5 | CONCLUSION

An efficient and robust method for inverse design of elastic rods is significant in a variety of research fields. Inspired by the internal mechanical link among edges of a rod, the bottom-up design method is proposed, which is capable of finding the optimal original shape for 2D clamped-free rods effectively. A searching algorithm is proposed and proved to be valid in searching the global minimum of the error function between the true undeformed curve and the candidate solutions. Excellent agreements are usually found between the designed deformed and target rods. The reason behind lack of good agreement in some cases is explained using the nondimensional parameter $\Delta l/L_{gb}$. The bottom-up design method can provide potential insights into real-world manufacturing of flexible objects (e.g., soft toys) and selection of suitable materials.

ACKNOWLEDGMENT

This work was funded by Natural Science Foundation of Jiangsu Province under Grant No. BK20210233 and Open Foundation of the State Key Laboratory of Fluid Power and Mechatronic Systems.

CONFLICT OF INTEREST

The authors declare no potential conflict of interests.

AUTHOR CONTRIBUTIONS

Longhui Qin: Conceived the presented idea and proposed the inverse design method, wrote and improved the manuscript. **Jianxiong Zhu:** Contributed in the validation of the proposed method. **Weicheng Huang:** Developed the numerical simulation, wrote and improved the manuscript.

DATA AVAILABILITY STATEMENT

Most of the data can be found within this article. Therein the general curves generated for validation of the proposed method is produced in random. They are available on request from the corresponding author. The data used for validation of special curves can be conveniently reproduced with Equations (17) to (20) and Table 1.

ORCID

Longhui Qin  <https://orcid.org/0000-0003-0070-8650>

Weicheng Huang  <https://orcid.org/0000-0001-9128-6099>

REFERENCES

1. Baranello L, Levens D, Gupta A, Kouzine F. The importance of being supercoiled: how DNA mechanics regulate dynamic processes. *Biochim Biophys Acta Gene Regul Mech BBA-Gene Regul Mech.* 2012;1819(7):632-638.
2. McMillen T, Goriely A. Tendril perversion in intrinsically curved rods. *J Nonlinear Sci.* 2002;12(3):241-281.
3. Bertails F, Audoly B, Cani MP, Querleux B, Leroy F, Lévéque JL. Super-helices for predicting the dynamics of natural hair. *ACM Trans Graph.* 2006;25(3):1180-1187.
4. Dong X, Raffles M, Guzman SC, Axinte D, Kell J. Design and analysis of a family of snake arm robots connected by compliant joints. *Mech Mach Theory.* 2014;77:73-91.
5. Klapper I. Biological applications of the dynamics of twisted elastic rods. *J Comput Phys.* 1996;125(2):325-337.
6. Dixit S, Singh-Zocchi M, Hanne J, Zocchi G. Mechanics of binding of a single integration-host-factor protein to DNA. *Phys Rev Lett.* 2005;94(11):118101.
7. Goyal S, Perkins NC, Lee CL. Nonlinear dynamics and loop formation in Kirchhoff rods with implications to the mechanics of DNA and cables. *J Comput Phys.* 2005;209(1):371-389.
8. Goriely A, Neukirch S. Mechanics of climbing and attachment in twining plants. *Phys Rev Lett.* 2006;97(18):184302.
9. Sander O. Geodesic finite elements for Cosserat rods. *Int J Numer Methods Eng.* 2010;82(13):1645-1670.
10. Kumar A, Steinmann P. A finite element formulation for a direct approach to elastoplasticity in special Cosserat rods. *Int J Numer Methods Eng.* 2021;122(5):1262-1282.
11. Roussel O, Renaud M, Taix M. Closed-forms of planar Kirchhoff elastic rods: application to inverse geometry. Proceedings of the IMA Conference on Mathematics of Robotics; 2015:9; Oxford, UK.
12. Prévost R, Whiting E, Lefebvre S, Sorkine-Hornung O. Make it stand: balancing shapes for 3D fabrication. *ACM Trans Graph.* 2013;32(4):1-10.
13. Wang G, Tao Y, Capunaman OB, Yang H, Yao L. A-line: 4D printing morphing linear composite structures. Proceedings of the 2019 CHI Conference on Human Factors in Computing Systems; 2019:1-12; IEEE.

14. Singh G, Krishnan G. Designing fiber-reinforced soft actuators for planar curvilinear shape matching. *Soft Robot.* 2019;7(1):109-121.
15. Turco E. Tools for the numerical solution of inverse problems in structural mechanics: review and research perspectives. *Eur J Environ Civ Eng.* 2017;21(5):509-554.
16. Wada H. Structural mechanics and helical geometry of thin elastic composites. *Soft Matter.* 2016;12(35):7386-7397.
17. Gazzola M, Dudte L, McCormick A, Mahadevan L. Forward and inverse problems in the mechanics of soft filaments. *R Soc Open Sci.* 2018;5(6):171628.
18. Lazarus A, Miller JT, Metlitz MM, Reis PM. Contorting a heavy and naturally curved elastic rod. *Soft Matter.* 2013;9(34):8274-8281.
19. Su T, Liu J, Terwagne D, Reis PM, Bertoldi K. Buckling of an elastic rod embedded on an elastomeric matrix: planar vs. non-planar configurations. *Soft Matter.* 2014;10(33):6294-6302.
20. Derouet-Jourdan A, Bertails-Descoubes F, Thollot J. Stable inverse dynamic curves. *ACM Trans Graph.* 2010;29(6):1-10.
21. Majumdar A, Goriely A. Static and dynamic stability results for a class of three-dimensional configurations of Kirchhoff elastic rods. *Phys D Nonlinear Phenom.* 2013;253:91-101.
22. Derouet-Jourdan A, Bertails-Descoubes F, Daviet G, Thollot J. Inverse dynamic hair modeling with frictional contact. *ACM Trans Graph.* 2013;32(6):1-10.
23. Zhang X, Yang J. Inverse problem of elastica of a variable-arc-length beam subjected to a concentrated load. *Acta Mech Sin.* 2005;21(5):444-450.
24. Hinkle AR, Goyal S, Palanthandlam-Madapusi HJ. Constitutive-law modeling of microfilaments from their discrete-structure simulations—A method based on an inverse approach applied to a static rod model. *J Appl Mech.* 2012;79(5):051005.
25. Chen X, Zheng C, Xu W, Zhou K. An asymptotic numerical method for inverse elastic shape design. *ACM Trans Graph.* 2014;33(4):1-11.
26. Fachinotti VD, Cardona A, Jetteur P. Finite element modelling of inverse design problems in large deformations anisotropic hyperelasticity. *Int J Numer Methods Eng.* 2008;74(6):894-910.
27. Bertails-Descoubes F, Derouet-Jourdan A, Romero V, Lazarus A. Inverse design of an isotropic suspended Kirchhoff rod: theoretical and numerical results on the uniqueness of the natural shape. *Proc Royal Soc A Math Phys Eng Sci.* 2018;474(2212):20170837.
28. Bergou M, Wardetzky M, Robinson S, Audoly B, Grinspun E. Discrete elastic rods. *ACM Trans Graph.* 2008;27:63.
29. Bergou M, Audoly B, Vouga E, Wardetzky M, Grinspun E. Discrete viscous threads. *ACM Trans Graph.* 2010;29:116.
30. Jawed MK, Novelia A, O'Reilly OM. *A Primer on the Kinematics of Discrete Elastic Rods.* Springer; 2018.
31. Turco E. Discrete is it enough? The revival of Piola-Hencky keynotes to analyze three-dimensional Elastica. *Contin Mech Thermodyn.* 2018;30(5):1039-1057.
32. Turco E, Barchiesi E, Giorgio I, Dell'Isola F. A Lagrangian Hencky-type non-linear model suitable for metamaterials design of shearable and extensible slender deformable bodies alternative to Timoshenko theory. *Int J Non-Linear Mech.* 2020;123:103481.
33. Qin L, Huang W, Du Y, Zheng L, Jawed MK. Genetic algorithm-based inverse design of elastic gridshells. *Struct Multidiscip Optim.* 2020;62(5):2691-2707.
34. Khadilkar MR, Paradiso S, Delaney KT, Fredrickson GH. Inverse design of bulk morphologies in multiblock polymers using particle swarm optimization. *Macromolecules.* 2017;50(17):6702-6709.
35. Tiow W, Yiu KFC, Zangeneh M. Application of simulated annealing to inverse design of transonic turbomachinery cascades. *Proc Inst Mech Eng A J Power Energy.* 2002;216(1):59-73.
36. Jawed MK, Da F, Joo J, Grinspun E, Reis PM. Coiling of elastic rods on rigid substrates. *Proc Natl Acad Sci.* 2014;111(41):14663-14668.
37. Singh R, Abhishek D, Kumar A. An asymptotic numerical method for continuation of spatial equilibria of special Cosserat rods. *Comput Methods Appl Mech Eng.* 2018;334:167-182. doi:10.1016/j.cma.2018.01.048
38. Li X, Huang W, Jawed MK. A discrete differential geometry-based approach to numerical simulation of Timoshenko beam. *Extreme Mech Lett.* 2020;35:100622. doi:10.1016/j.eml.2019.100622
39. McKinley S, Levine M. Cubic spline interpolation. *College Redwoods.* 1998;45(1):1049-1060.
40. Burchitz I, Meinders T. Adaptive through-thickness integration for accurate springback prediction. *Int J Numer Methods Eng.* 2008;75(5):533-554.
41. Tam D, Radovitzky R, Samtaney R. An algorithm for modelling the interaction of a flexible rod with a two-dimensional high-speed flow. *Int J Numer Methods Eng.* 2005;64(8):1057-1077.

SUPPORTING INFORMATION

Additional supporting information may be found online in the Supporting Information section at the end of this article.

How to cite this article: Qin L, Zhu J, Huang W. A bottom-up optimization method for inverse design of two-dimensional clamped-free elastic rods. *Int J Numer Methods Eng.* 2022;123(11):2556-2572. doi: 10.1002/nme.6950